Study of voids in chilled samples of magnesium treated irons

Haruki Itofuji*

Technical Development Sec., Ube Steel Co., Ltd, 1978-19 Okinoyama, Kogushi, Ube City, Yamaguchi Pref. 755-0067 Japan

Chilled samples of base iron and magnesium-treated iron were surveyed using optical microscopy, SEM and computer assisted microanalysis. Numerous voids, 0·5–1 μm in size, were observed in magnesium-containing chilled samples. Graphite spheroids at an early stage of growth, 3–5 μm in size, and inclusions were also observed. Voids were not found in the base iron samples but inclusions were observed. Magnesium enrichment was detected at the voids, graphite and inclusions of the magnesium treated samples. It is proposed that the voids represent the traces of magnesium vapour bubbles formed in the melt. Some graphite spheroids consist of a thin graphite layer at their surface and a hollow core, a morphology that supports nucleation on the void walls followed by growth towards the centre. Although inclusions were occasionally observed in the centres of graphite spheres, they do not appear to be essential for spheroidisation to occur. It is concluded that gas bubbles formed by free magnesium contribute to the formation of spheroidal graphite by supplying nucleation and growth sites. IJCMR/358

 Manuscript received 21 November 2000; accepted 28 July 2004.

Keywords: Spheroidal graphite iron; Spheroidization theory; Mg gas bubble; CMA analysis

Introduction

Residual magnesium is widely used to control nodule quality in ductile iron production. However, there are considerations beyond residual magnesium level, since magnesium exists in ductile iron in both metallic and non-metallic states. In the following, these states are termed free magnesium and inclusive magnesium, respectively. The present author has concluded that free magnesium is the key state, whereas inclusive magnesium has no influence on spheroidal graphite formation.[1] However, other researchers[2–4] have concluded that magnesium containing inclusions act as nuclei for spheroidal graphite formation, while free magnesium controls their further growth, although the role of free magnesium in this process remains to be clarified. Knowledge of the mechanism controlling spheroidal graphite formation is important for engineers and foundrymen.

The flow chart in Fig. 1 shows how free magnesium contributes to spheroidal graphite formation and becomes distributed within the graphite body. To distinguish graphite nodules at the early and late stage of the formation process, the initial form of spheroidal graphite is termed sphere graphite in Fig. 1 and in the discussion below. This rationale has been constructed on the basis of site theory.[5] Evidence in support of most stages of the mechanism proposed in Fig. 1 has been presented previously.[1,5–10] The present study puts forward evidence from analyses of magnesium-containing chilled samples to support the steps within the dashed rectangles in the flow chart. Magnesium will vaporise in liquid iron because of its low boiling point (~1100°C, Ref. 11). Vaporised magnesium is likely to exist in the form of gas bubbles, since magnesium has almost no solubility in liquid iron,[6] and indeed boiling and bubbling phenomena are observed when magnesium alloy is added to liquid iron in practice. The solubility of magnesium in solid iron is also very low.[6] Therefore, if magnesium-treated liquid iron were rapidly solidified in a metal mould, the magnesium gas bubbles will be frozen as voids between quenched phases. In the present study, the distribution and morphology of free magnesium in the chilled sample is examined, and the relationship between these results and spheroidal graphite formation is discussed.

Experimental procedure

Melting and sampling were carried out under industrial conditions. Base iron was melted in a 10 t low frequency induction furnace. After adjusting the chemical composition and superheating to over 1500°C, the iron was poured into a metal mould to produce chilled samples for testing. Tapping was conducted at 1434°C. A similar 10 t base iron melt was treated with Fe–Si–5·5Mg and Fe–75Si by the sandwich method (compositions are mass percentages unless indicated otherwise). A chilled sample of the treated iron was obtained by the same method after the magnesium reaction was complete. The residual liquid iron was poured into the mould employing normal foundry practice. No problems were encountered with the quality of the commercial castings.

Samples were analysed using an emission spectrometer in conjunction with a pulse-height dispersive analysis (PDA) system. A state analysis[1] was also conducted for magnesium using the same emission spectrometer. Analytical results are summarised in Table 1.

The analysed surfaces were also characterised by optical and scanning electron microscopy [both

*Email, h-itofuji@mx5.tiki.ne.jp

 DOI 10.1179/136404604225022658

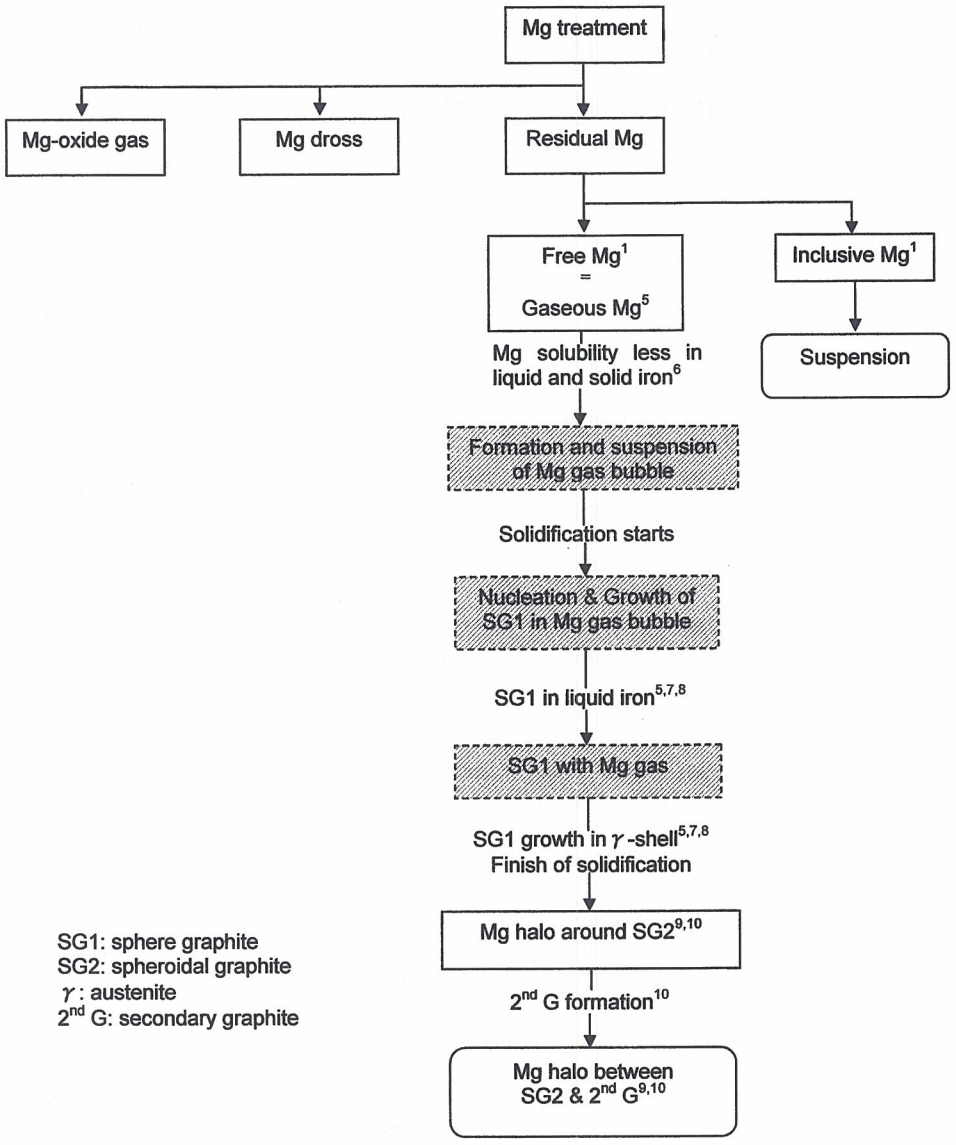

1 Flow chart of role of magnesium in spheroidal graphite formation on basis of site theory: cross-hatched boxes with dashed lines indicate areas discussed in present study

thermal and field emission (FE) SEM] and computer-aided electron probe microanalysis (CMA). The chilled samples were rough polished with emery paper, rinsed with water, and then finished by polishing with diamond paste suspended in polishing oil. After polishing, the chilled samples were cleaned with acetone, rinsed with alcohol and dried with a blower. Initially, the chilled samples were examined in the unetched condition. After characterisation as described above, the chilled samples were etched with 2% nital to facilitate identification of the phases present in the chill microstructure.

Table 1 Chemical composition of chilled samples, mass-%

	C	Si	Mn	P	S	Total Mg	Free Mg
Base iron	3·52	1·43	0·14	0·031	0·019	0·0000	0·0000
Mg-treated iron	3·49	2·41	0·16	0·031	0·014	0·0500	0·0425

Results

Optical microstructures of magnesium containing samples are shown in Fig. 2. To optimise imaging of the distribution of black spots, the microstructures were taken at a magnification of 1000×; therefore, a montage of three photos is required to cover the same area as the CMA analyses discussed below. A large number of black spots, ~1 μm or less in size, were observed in the unetched microstructure (Fig. 2*a*). Many examples of sphere graphite were also observed. These were 3–5 μm in size and occurred more frequently in the central area of the sample than in the peripheral areas. This sphere graphite is considered to represent an initial growth morphology of spheroidal graphite. The black spots are located at the interfaces in the etched microstructure (Fig. 2*b*), e.g. between primary austenite dendrites and eutectic ledeburite and between ledeburite austenite and cementite.

Figure 3 is a SEM image of the area shown in Fig. 2. From secondary electron imaging, the black

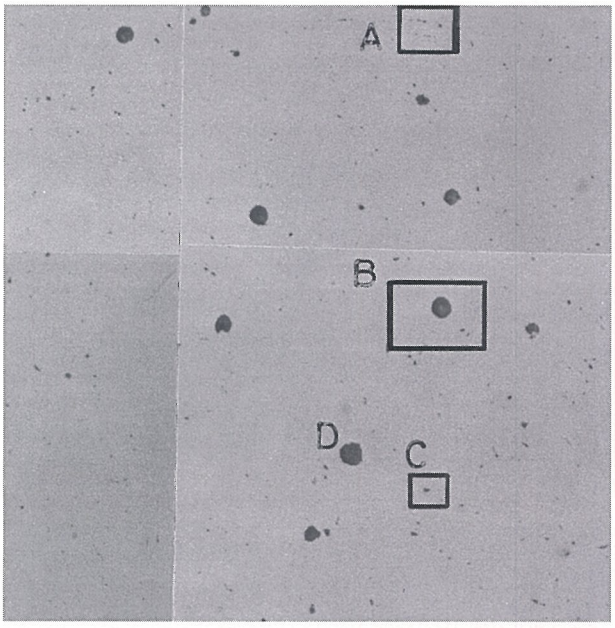

a unetched; *b* etched in 2% nital after CMA analysis

2 Optical microstructures of same area of magnesium-containing chilled sample

spots were judged to be voids in the matrix structure. However, clear resolution in micrographs was difficult because the conventional SEM had poor depth resolution. A specific area was therefore also observed using FE-SEM, which can detect microscale surface roughness. To utilise the full capability of FE-SEM, the magnesium-containing sample was tilted at 30° to the electron beam rather than the conventional perpendicular (0°) orientation.

Most of the black spots could clearly be identified as micro-voids that are totally different in size and morphology from the micro-voids and shrinkage cavities commonly observed; examples are shown in Fig. 4 (the images relate to the areas marked A, B and C in Fig. 2). Some of the black spots observed were

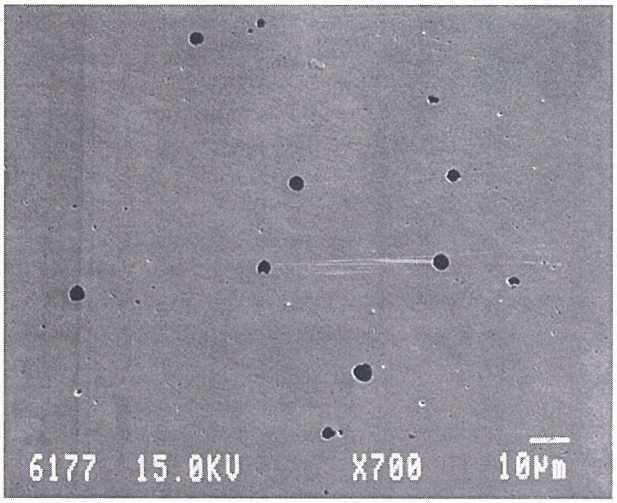

3 Scanning electron micrograph of unetched Mg-treated sample after CMA analysis

inclusions. These were of two types: rectangular Mg–Si–Al–N and spherical Mg–Ca–S particles. Both were 0·5–1·0 μm in size (Fig. 5). Inclusions were only rarely observed to be associated with sphere graphite. If samples were observed only in the etched condition, the existence of voids might be overlooked.

In the base iron sample, spherical Al–Si–Ca inclusions were observed but sphere graphite and voids were not.

Magnesium distribution was analysed in the microstructure shown in Fig. 3, using CMA in conjunction with colour mapping. The brighter square represents the exact area analysed. The results are shown in Fig. 6. An electron beam diameter of 0·26 μm was selected for void, inclusion and sphere graphite. The other conditions for analysis are printed in the figure. These conditions were optimised for the chill microstructure during pretrial studies. The magnesium map shown in Fig. 6*a* corresponds closely with the black spots in Fig. 2*a*. This suggests that magnesium was concentrated at the voids, sphere graphite and inclusions; no magnesium was detected in the matrix structure. This confirms the very low solubility of magnesium in liquid and solid iron predicted by the magnesium–iron equilibrium phase diagram.

Although the intensity of the characteristic X-rays was strongest from the inclusions, no inclusions were observed within any of the sphere graphite bodies in the analysed area. However, inclusions were observed at a small number of graphite spheres in the other areas; in these cases, graphite nodularity was poor – even if the inclusions were spherical, the graphite was not truly so. An example is shown in Fig. 7, in which the inclusion was about 1·8 μm in size. Although several surveys were conducted, only sphere graphite in area D in Fig. 2*a* was found to be almost completely magnesium free.

In an attempt to map precisely the segregation of magnesium in the chill microstructure, a colour map of the eutectic ledeburite skeleton was produced from the unetched sample. Silicon is the best element to

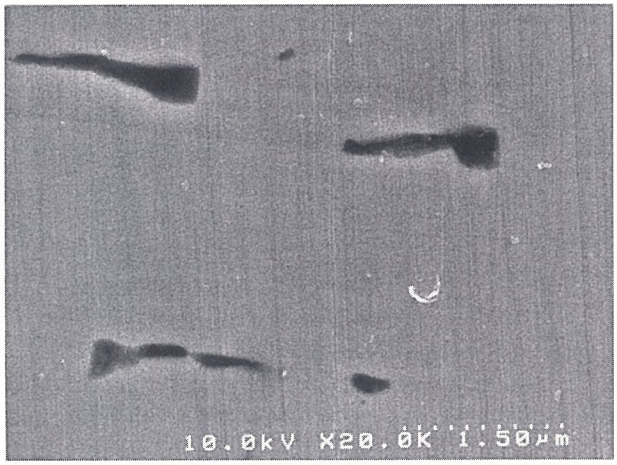

(a)

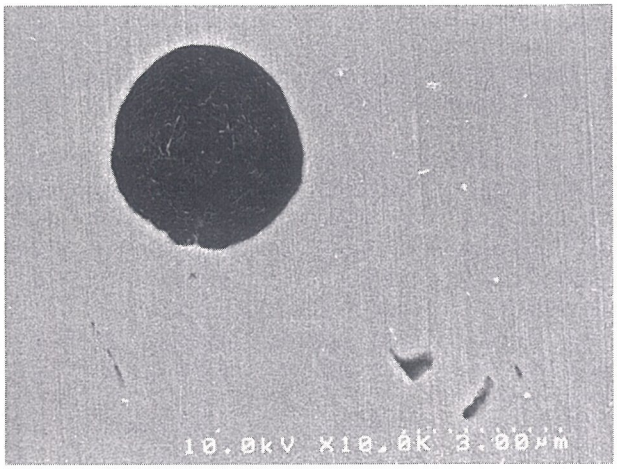

(b)

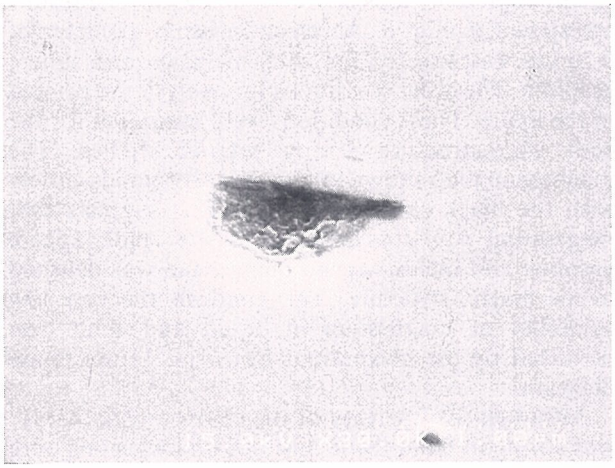

(c)

a between directional ledeburite structures (location A in Fig. 2); *b* near sphere graphite (location B in Fig. 2); *c* between austenite dendrites (location C in Fig. 2)

4 Voids observed in Mg-treated sample (FE-SEM, tilt 30°)

define this structure since ledeburitic cementite shows no intensity for silicon, whereas primary and ledeburitic austenite do. A good ledeburite skeleton could be identified in the silicon map of the chilled sample. The silicon and magnesium maps were combined by computer (Fig. 6*b*). The correlation

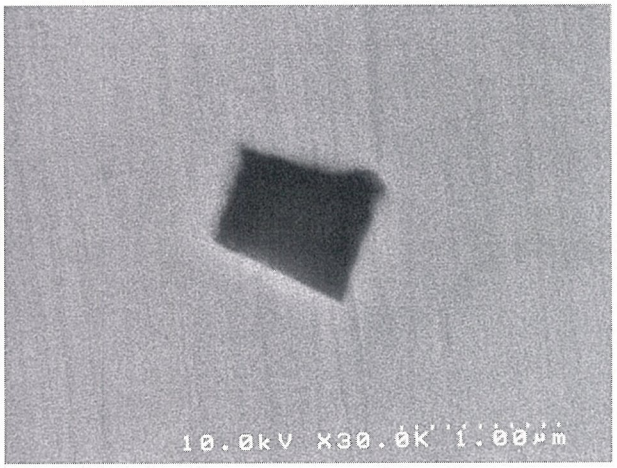

(a)

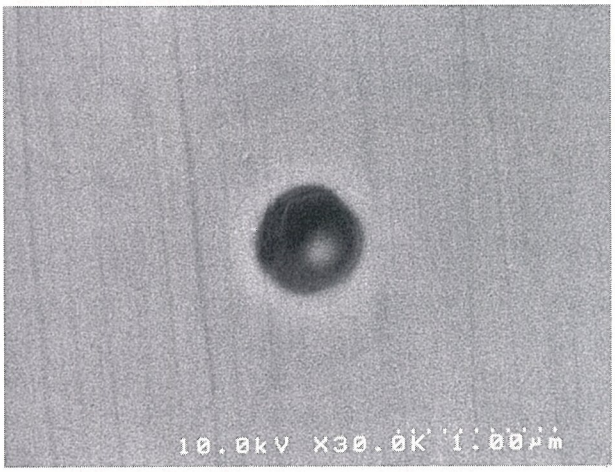

(b)

a Mg–Si–Al–N system; *b* Mg–Ca–S system

5 Inclusions in Mg-treated chill sample (FE-SEM, tilt 35°)

between the elemental map and the microstructure can be described as follows:

(i) Mg–Si area: primary and ledeburitic austenite with sphere graphite, voids and inclusions
(ii) Mg area: sphere graphite, voids and inclusions
(iii) Si area: primary and ledeburitic austenite
(iv) black area: ledeburite cementite.

As would be expected, the graphite microstructure inferred in Fig. 6*b* matches the real microstructure in Fig. 2*b*. In Fig. 6*b*, magnesium can be seen to be concentrated at sphere graphite, inclusions and the interfaces between primary austenite, ledeburitic austenite and ledeburitic cementite. Voids also occurred at these interfaces, which implies that magnesium has no solubility in either liquid or solid iron.

To survey the relationship between voids and graphite nucleation and growth, the sphere graphite was observed in detail using FE-SEM. Typical results are shown in Fig. 8. The sphere graphite could be roughly divided into three types:

(i) a few graphite spheres had hollow bodies and layers consisting of thin graphite chips were observed on the walls of the voids (previous studies[5,7,8] have shown the substructure of

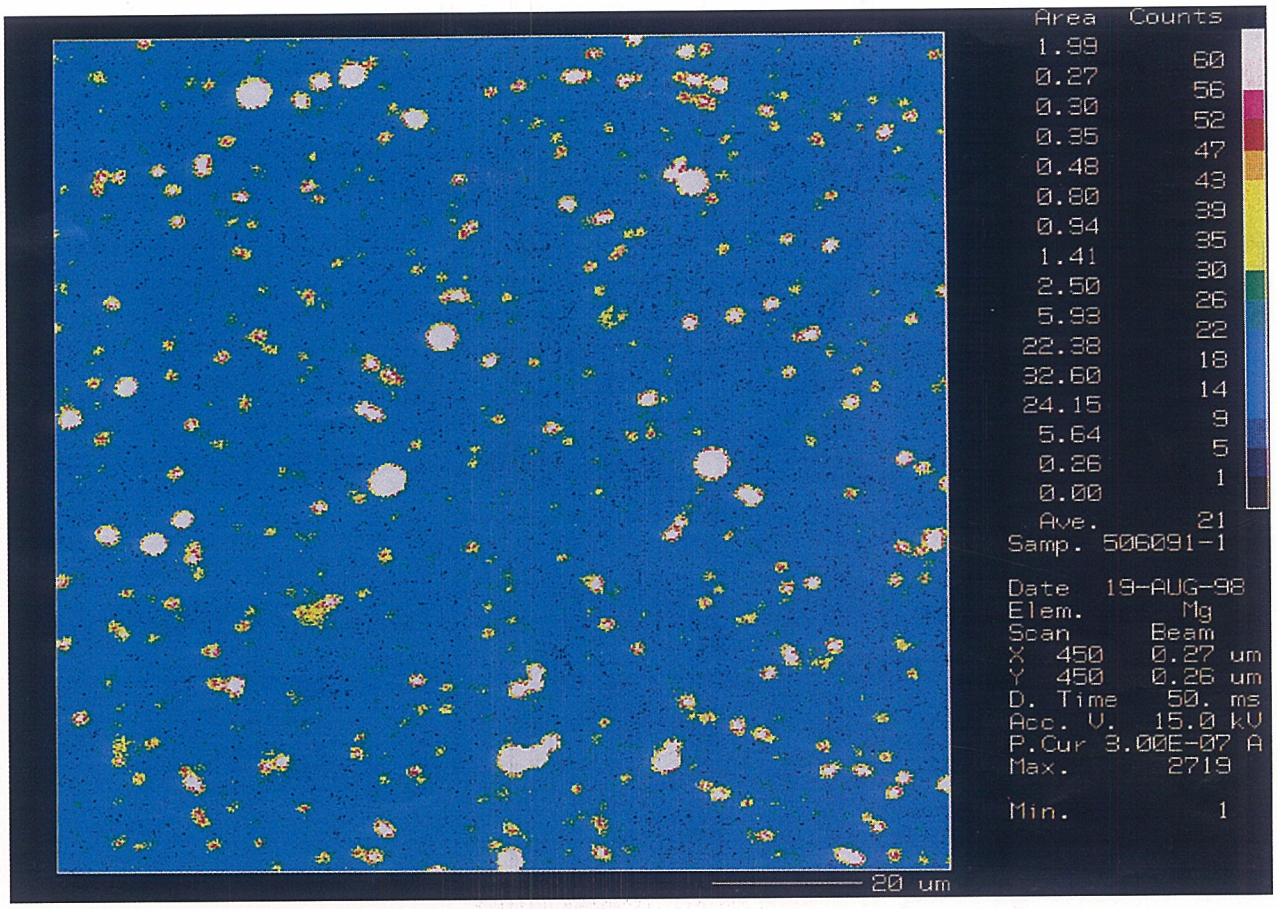

(a)

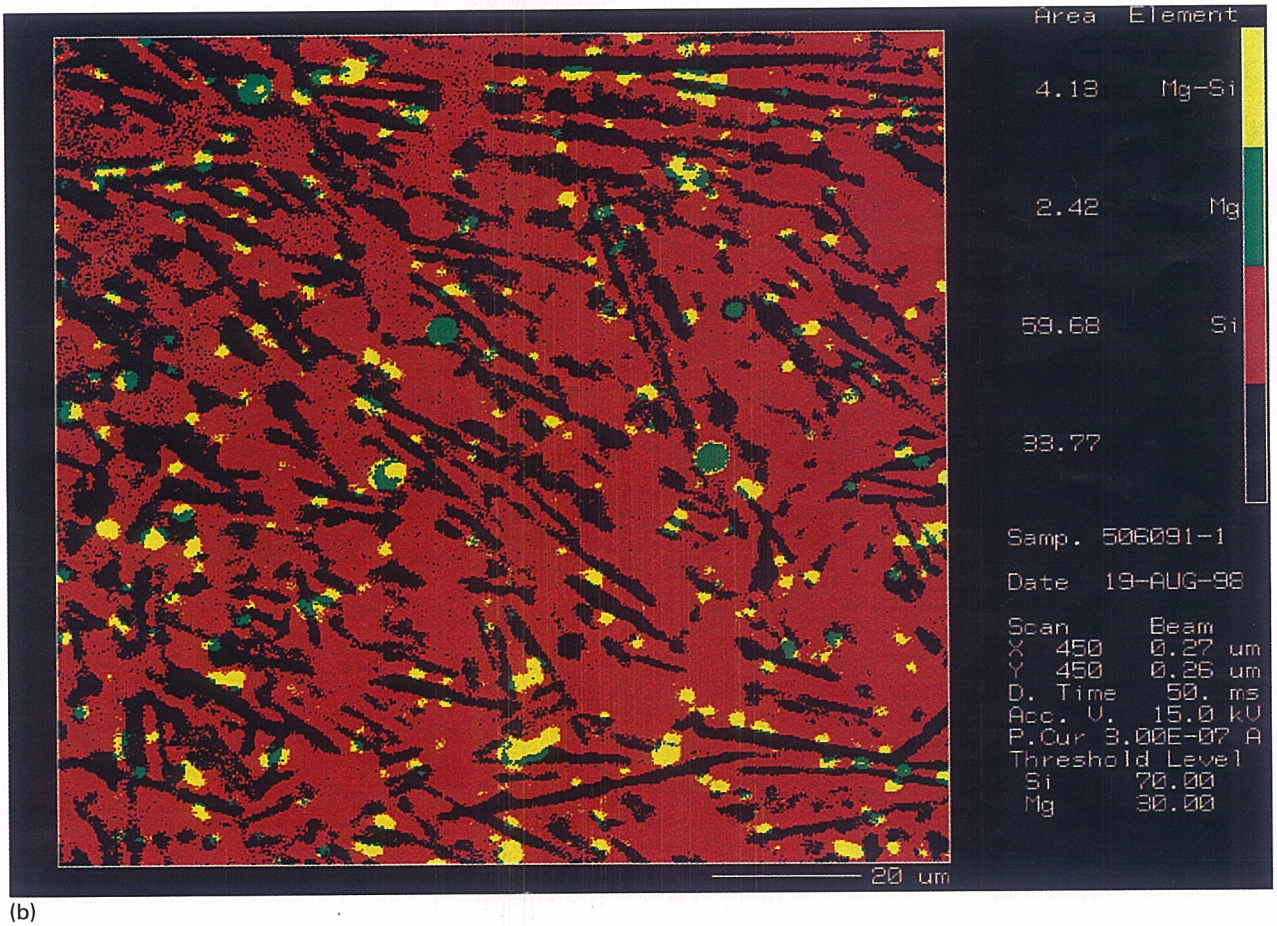

(b)

a Mg; *b* Mg–Si

6 CMA maps of microstructure in Fig. 2

7 Sphere graphite containing magnesium (Mg–Ca–Ce–S) inclusion (FE-SEM): observed in same sample but different area from Fig. 6

spheroidal graphite to consist of layers of thin graphite chips)

(ii) some spheres were partially hollow, having no graphite at their core

(iii) most commonly, the spheres were completely composed of solid graphite.

These phenomena suggest that sphere graphite may nucleate at the walls of voids and grow towards the centre. If the voids are formed by magnesium gas bubbles, they would have to have spherical shapes in the solid iron. However, in this chilled sample, a number of non-spherical voids were observed. This will be discussed below.

Discussion

In a recent paper,[1] a mechanism was proposed in which the presence of free magnesium is indispensable for graphite spheroidisation in irons, and evidence to support this has been put forward. This new concept is based on site theory.[5] As mentioned above, because of its poor solubility and physical properties,[6,11] free magnesium is considered to exist in liquid iron as bubbles of magnesium vapour. The pressure within the bubble will match the hydrostatic pressure of the liquid iron. Since magnesium has almost no solubility in solid iron either, the bubbles would be expected to remain as voids following solidification.

In the present study, many voids were observed in the magnesium-containing chilled sample, and segregation of magnesium to the sites of these voids was detected. Magnesium might segregate at the surfaces of voids. No voids were observed in chilled sample of the base iron from the same charge. Although magnesium-treated iron is more prone to microshrinkage porosity than untreated iron, the voids observed in the present study were completely different from such porosity in situation and dimension. Microshrinkage porosity occurs in the areas that are last to solidify; the present voids, however, were distributed throughout the chilled sample. The porosity is typically 1 mm in size, whereas the voids were 1 μm or less. It is considered unlikely that the voids in the magnesium containing chilled sample are

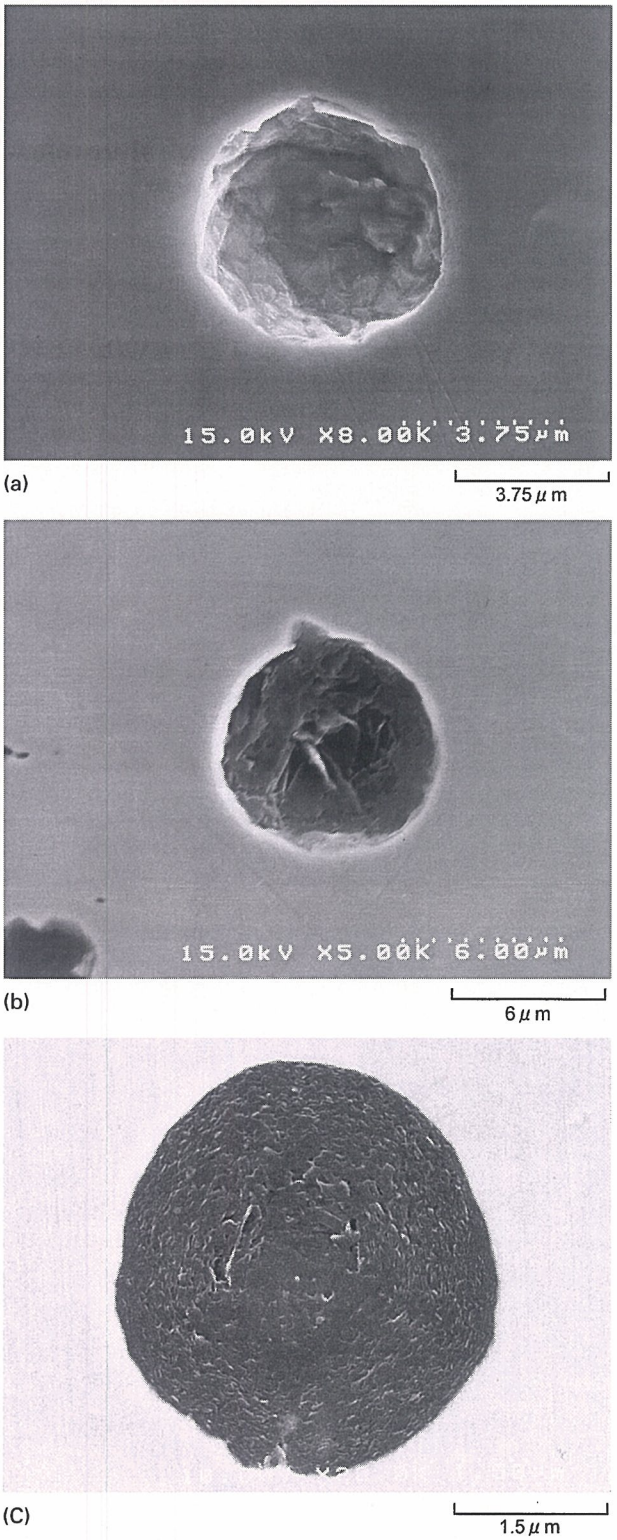

a initial stage (graphite chips on wall of void); *b* intermediate stage (centre still hollow); *c* final stage (void is filled with graphite)

8 Growth of sphere graphite in Mg-treated chill sample (FE-SEM)

microshrinkage porosity, whereas it is reasonable to associate them with traces of magnesium vapour bubbles.

Ohide[12] has provided evidence for the existence of magnesium gas bubbles in liquid iron. In this work, magnesium-treated and untreated iron, poured into the same mould cavity at the same time, separated

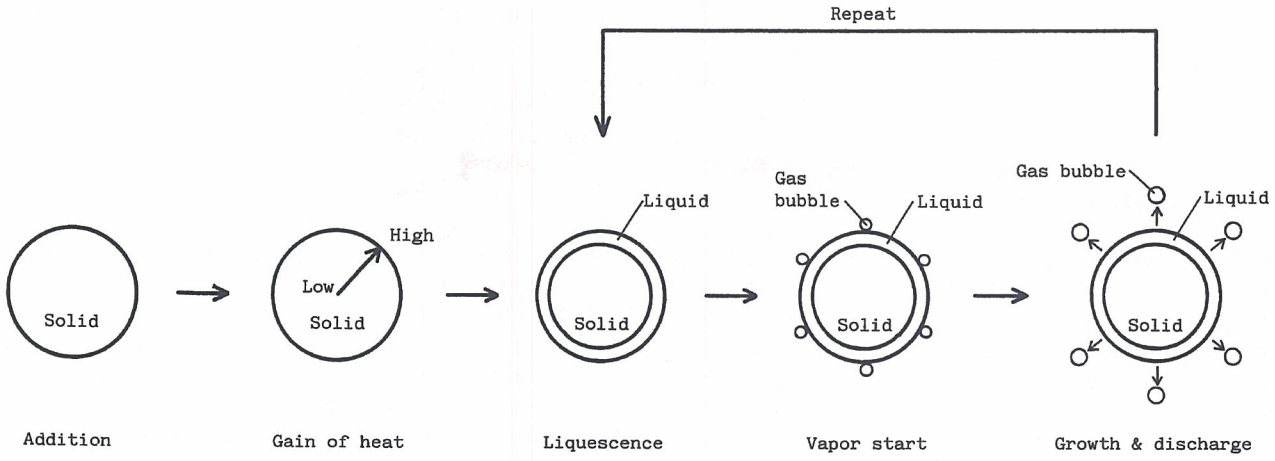

9 Mechanism of magnesium vapour bubble formation in liquid iron[5]

into two liquid layers, although partial mixing occurred at the boundary. The magnesium-treated iron always formed the upper layer, an effect attributed to the fact that the presence of magnesium vapour bubbles lowers the density relative to untreated liquid iron.

The size of magnesium gas bubbles in liquid iron can be calculated as

$$P_{Mg} = P_a + \rho gh + 2\gamma/r \quad \ldots\ldots\ldots (1)$$

where[13]

$$\log P_{Mg} = 4{\cdot}958 - (1{\cdot}229 \times 10^4)/T \quad \ldots\ldots (2)$$

Here, P_{Mg} is the vapour pressure of magnesium, P_a atmospheric pressure (=1 atm), ρ the density of liquid iron (6·8 g cm^{-3} at 1400°C, Ref. 14), g the acceleration due to gravity (980 cm s^{-2}), h the head of liquid iron (1–100 cm), γ the surface tension of liquid iron (1·450 J m^{-2} at 1410°C, Ref. 15), r the bubble radius (cm) and T the Rankine (absolute Fahrenheit) temperature of liquid iron.

1450 dyn/cm

It can be seen that r is most strongly determined by the vapour pressure of magnesium following treatment. Calculated diameters at several temperatures and depths are given in Table 2. According to the same calculation, the bubble diameter for iron treated with Fe–Si–5·5Mg at 1434°C was estimated as 7–8 μm.

The proposed mechanism for formation of bubbles caused by the vaporisation of magnesium in liquid iron[5] is illustrated in Fig. 9. It is proposed that magnesium alloys undergo localised vaporisation by surface boiling.[16]

Since the voids in the chilled iron are traces of magnesium bubbles, they should be spherical. However, the voids observed in the chilled sample were rectangular in cross-section and about 1 μm in size. It is proposed that the bubbles become entrapped at interfaces in the rapidly solidifying structure and are subsequently deformed by solidification stresses. Thus, the vapour pressure of magnesium may be reduced and liquation may occur around the time that the solidification of eutectic cementite is completed. Under those conditions, the form of the magnesium vapour bubbles might be changed. However, it is proposed that bubbles could retain their original spherical form if graphite precipitation has occurred within the cavity. Evidence of graphite formation within voids is shown in Fig. 8*a* and *b*. Some examples of sphere graphite had a few graphite layers on the void walls (Fig. 8*a*), whereas others had low graphite density at the centre of the sphere (Fig. 8*b*). It is considered that these spheres were preserved at an early stage of growth by quenching, supporting the contention that sphere graphite is an initial form of spheroidal graphite which is nucleated on the wall of magnesium vapour bubbles and grows inwards towards the centre.

Yamamoto *et al.*[17] and Kasperek and Tellier[18] have reported the existence of spheroidal graphite with a hollow core. The spheroidal graphite in this study had a thicker graphite layer and smaller hollow core, and

Table 2 Calculated diameter of magnesium vapour bubbles in liquid iron treated with magnesium spheroidising agent

Treatment temperature, °C	Vapour pressure, atm	Bubble diameter at liquid depth D, μm			
		D=1 cm	D=10 cm	D=100 cm	D=500 cm
1200	2·1	49	51	108	*
1300	4·2	17	17	21	*
1350	5·6	12	12	13	40
1400	7·6	8	8	9	16
1450	10·0	6	6	6	9
1500	12·9	4	5	5	6
1600	20·7	3	3	3	3

*Cannot exist as bubble in liquid iron.

10 Nucleation and growth mechanism of graphite in magnesium vapour bubble[5,7,8]

did not provide sufficient evidence to confirm the nucleation and growth behaviour of spheroidal graphite. However, the present FE-SEM micrographs of thin graphite layers on the wall of voids originating from magnesium vapour bubble provide firmer evidence. The mechanism of graphite nucleation and growth in magnesium vapour bubbles[5,7,8] is schematically illustrated in Fig. 10. Strong evidence for the subsequent growth behaviour of sphere graphite has been presented previously[6–8] and is illustrated in Fig. 11.[5,8,9,19] Successive thin layers of graphite build up within the austenite shell to produce the familiar spheroidal graphite morphology. However, a spheroidal 'template' is required to generate spheroidal growth. Spheroidal graphite is therefore frequently formed from thin graphite chips in which the plate surface is the basal plane of the hexagonal graphite crystal structure. The same mechanism applies for spheroidal graphite formation in the solid state during tempering heat treatment.[20,21] Special morphologies,[22–25] e.g. spirals, cone helixes, circumferential and fullerene type growth, influencing the growth form of spheroidal graphite had not been observed in the present work. However, it is possible that some graphite nodule surfaces, observed under the poor surface roughness resolution of conventional SEM, could appear to provide evidence of these growth modes.

The sphere graphite observed was all 3–5 μm in size: reasonably close to the calculated size of magnesium vapour bubbles in liquid iron under the present experimental conditions. If the diameter of the magnesium gas bubble is presumed to be 8 μm, the flotation rate U in liquid iron would be 0·22 cm min^{-1} according to Stokes law

$$U=[2r^2(\rho_l-\rho_{Mg})g]/9\eta \quad . \quad . \quad . \quad . \quad . \quad . \quad . \quad . \quad . \quad (3)$$

where ρ_l (=6·8 g cm^{-3}, Ref. 14) and ρ_{Mg} (~0) are the densities of liquid iron and magnesium vapour and η is the viscosity of liquid iron (=0·05 g cm^{-1} s^{-1} at 1430°C, Ref. 26).

Under such conditions, if the height of liquid iron were 10 cm, the maximum suspension time of a magnesium gas bubble would be 36 min. This matches well the fading time of magnesium previously reported by many researchers.[27] One magnesium fading phenomenon is the floating and escape of magnesium vapour bubbles from liquid iron.

Magnesium-containing inclusions were also observed in the treated sample. The inclusions were less numerous than the voids and a few inclusions co-located with sphere graphite were observed. The inclusions were 0·5–1·0 μm in size, in contrast to the 3–5 μm diameter of the sphere graphite. If inclusions act as nuclei for graphite spheroidisation, it would be expected that many inclusions would have been detected by FE-SEM and/or CMA within the sphere graphite. However, this was not the case.

It is therefore proposed that inclusions do not directly contribute to the nucleation and growth of spheroidal graphite. The interfaces between inclusions and liquid iron may act as a nucleation and growth site for graphite, but not for spheroidal graphite. Further, there is currently no mechanism whereby inclusions can influence the final morphology and substructure of spheroidal graphite.[8] The presence of inclusions in graphite nodules can, it is proposed, be explained by their entrapment within

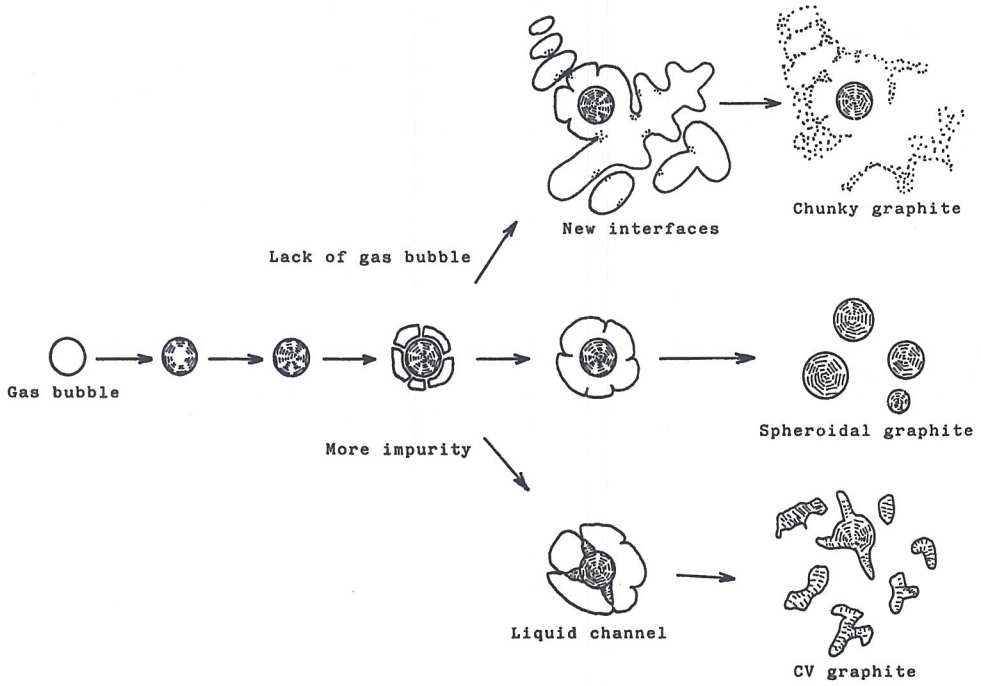

11 Schematic illustration of graphite formation in liquid iron treated with spheroidising agent[5,8,9,19]

magnesium vapour bubbles. Graphite would then nucleate and grow inwards in the manner shown in Fig. 10, trapping the inclusion within the spheroid.[5,7–9] It has already been shown that a magnesium halo (considered to be the trace of a magnesium vapour bubble) exists around spheroidal graphite, whether or not the spheroid has an inclusion at its core.[5,8–10]

Many researchers have reported that spheroidal graphite nucleates on magnesium-containing inclusions. However, the subsequent role of free magnesium in controlling the growth morphology of spheroidal graphite remains unclear.

Although sphere graphite having almost no magnesium segregation was observed in the present study, this graphite could have nucleated and grown within other types of gas bubble formed in liquid iron. This supposition is supported by the experimental results of Yamamoto *et al.*,[17] who have concluded that nitrogen, carbon dioxide and argon could nucleate spheroidal graphite if fine gas bubbles can be introduced into, and retained in, liquid iron. Under rapid solidification conditions, the formation of gas bubbles consisting of non-spheroidising elements could be feasible. These gas bubbles are different from the shrinkage porosity occurring during solidification.

Conclusions

1. Many voids were observed in the magnesium-treated chilled iron sample whereas no voids were observed in the base sample. Both samples were prepared using standard industrial practice.
2. Sphere graphite, considered to be an initial form of spheroidal graphite, and inclusions were also found in the magnesium-treated chilled sample.
3. Magnesium was detected by CMA in the inclusions and the spheres and voids, but not in the iron matrix.
4. It is proposed on the basis of this and micrographic evidence that sphere graphite nucleates on the walls of voids and grows inwards.
5. There is a high probability that the voids observed represent traces of bubbles of magnesium vapour formed in the melt.
6. It is concluded that magnesium gas bubbles are necessary for formation of sphere graphite, whereas inclusions are not.

Acknowledgements

The author thanks Mark Fields of Cast-Fab Technologies Inc. for his kind help in the writing of this paper and expresses appreciation to Chiaki Takano for her kind support.

References

1. H. ITOFUJI: *Int. J. Cast Met. Res.*, 1999, **12**, 179–187.
2. T. SKALAND, O. GRONG and T. GRONG: *Metall. Trans. A*, 1993, **24A**, 2321–2345.
3. C. R. LOPER JR, R. C. VOIGT, J. R. YANG and G. X. SUN: *Trans. AFS*, 1981, **89**, 529.
4. H. NAKAE, Y. IGARASHI and Y. ONO: *J. Jpn Foundry Eng.*, 2001, **73**, 111.
5. H. ITOFUJI: *Trans. AFS*, 1996, **104**, 79–87.
6. T. B. MASSALSKI (ed.): 'Binary alloy phase diagrams', Vol. 2, 1722; 1992, Materials Park, OH, ASM International.
7. H. ITOFUJI: *AFS Trans.*, 1983, **91**, 313–324.
8. H. ITOFUJI: 'Study on graphite spheroidization in cast irons', doctorate degree thesis, Kyoto University, 1993
9. H. ITOFUJI: *Cast Metals*, 1992, **5**, 6–19; 235–238.
10. H. ITOFUJI: *Cast Metals*, 2001, **14**, 15–23.
11. 'Japan Institute of Metals data book', 10; 1974, Tokyo, Maruzen.
12. T. OHIDE: *Int. J. Cast Met. Res.*, 1997, **9**, 279–284.
13. P. K. TROJAN and R. A. FLINN: *Trans. ASM*, 1961, **54**, 549–566.
14. 'Japan Institute of Metals data book', 289; 1974, Tokyo, Maruzen.
15. K. LOHBERG and W. WUNDER: *Giesserei*, 1966, **18**, 189–196.
16. Y. I. NESIS: 'Boiling of liquids'; 1973, Moscow, Nauka.
17. S. YAMAMOTO, Y. KAWANO, B. CHANG and R. OZAKI: *AFS Trans.*, 1975, **83**, 217–226.
18. J. KASPEREK and J. C. TELLIER: *Mem. Etud. Sci. Rev. Metall.*, 1991, 654–661.
19. H. ITOFUJI and A. MASUTANI: *Int. J. Cast Met. Res.*, 2001, **14**, 1.
20. Y. LEE: 'Action of gas and vapor element on microstructural change in iron', doctoral thesis, Kyoto University, Japan, 1986.
21. K. HANAWA, K. AKECHI, Z. HARA and T. NAKAGAWA: *Trans. Jpn Inst. Met.*, 1980, **21**, 765.
22. A. A. NAFAL, L. A. EL-MANAWATI and M. A. WALI: Proc. 56th World Foundry Cong., Düsseldorf, Germany, May 1989, Paper 21.
23. Q. LIU and Q. LIU: *AFS Trans.*, 1993, **101**, 101.
24. B. MIAO, W. BIAN, K. FANG and M. H. FAN: *J. Mater. Sci.*, 1994, **29**, 255–261.
25. D. D. DOUBLE and A. HELLAWELL: *Acta Metall. Mater.*, 1995, **43**, 2435.
26. 'Handbook of physical properties for liquid iron and slag', 53; 1972, Tokyo, Japan Iron and Steel Institute.
27. B. CHANG, S. YAMAMOTO, Y. KAWANO and R. OZAKI: *J. Jpn Inst. Met.*, 1977, **41**, 1019–1025.